PAPER • OPEN ACCESS

Design and in-field testing of the world's first ReBCO rotor for a 3.6 MW wind generator

View the article online for updates and enhancements.

Design and in-field testing of the world's first ReBCO rotor for a 3.6 MW wind generator

Anne Bergen[1] , **Rasmus Andersen[2], Markus Bauer[3], Hermann Boy[4],
Marcel ter Brake[1], Patrick Brutsaert[5], Carsten Bührer[6], Marc Dhallé[1],
Jesper Hansen[2], Herman ten Kate[1], Jürgen Kellers[6], Jens Krause[6],
Erik Krooshoop[1], Christian Kruse[7], Hans Kylling[8], Martin Pilas[8],
Hendrik Pütz[6], Anders Rebsdorf[2], Michael Reckhard[9], Eric Seitz[10],
Helmut Springer[9], Xiaowei Song[2]** , **Nir Tzabar[1], Sander Wessel[1],
Jan Wiezoreck[6], Tiemo Winkler[1,3] and Konstantin Yagotyntsev[1]**

[1] University of Twente, 7522 NB Enschede, The Netherlands
[2] Envision Energy Aps, Silkeborg, DK-8600, Denmark
[3] Theva Dünnschichttechnik GmbH, D-85737 Ismaning, Germany
[4] Sumitomo (SHI) Cryogenics of Europe GmbH, Darmstadt, Germany
[5] Jeumont Electric, Jeumont, France
[6] Eco 5 GmbH, Bonn, Germany
[7] DNV GL Energy, D-20457 Hamburg, Germany
[8] Fraunhofer Institure for Wind Energy Systems, Bremerhaven, Germany
[9] Delta Energy Systems GmbH, D-59494 Soest, Germany
[10] Sumitomo (SHI) Cryogenics of America, Inc., Allentown, PA, United States of America

E-mail: a.bergen@utwente.nl

Abstract

The main aim of the EU H2020 project EcoSwing was to demonstrate a technical readiness level of 6–7 for high-temperature superconducting (HTS) technology operating in a wind generator. To reach this goal, a full-scale synchronous HTS generator was successfully designed, built and field-tested in a 3.6 MW turbine. The generator has a rotor with 40 superconducting coils of 1.4 m long. The required >20 km of coated conductor was produced within the project's time schedule. All coils were tested prior to assembly, with >90% of them behaving as expected. The technical readiness level of HTS coils was thus increased to level 7. Simultaneously, the maturing of cryogenic cooling technology over the last decade was illustrated by the several Gifford-McMahon cold-heads that were installed on-board the rotor and connected with the stationary compressors through a rotating coupling. The cryogenic system outperformed design expectations, enabling stable coil temperatures far below the design temperature of 30 K after only 14 d of cool-down. After ground-based testing at the IWES facility in Bremerhaven, Germany, the generator was installed on an existing turbine in Thyborøn, Denmark. Here, the generator reached the target power range and produced power for over 650 h of grid operation.

Keywords: superconducting machinery, HTS, wind turbine, superconducting generator

(Some figures may appear in colour only in the online journal)

1. Introduction

Wind turbine size has grown significantly over recent decades [1]. However, today's technology has trouble keeping up with this trend towards ever increasing unit power levels. Support

structures need to cope with the nacelle's mass, especially for direct-drive (DD) generators. Geared drivetrains have the advantage of being relatively lightweight, cost-efficient and proven, but are prone to gearbox failures [2]. Therefore, permanent-magnet (PM) based DD generators are presently a common solution in state-of-the-art multi-MW generators. Yet the feasibility of 10+ MW PM-DD turbines requires significant weight reduction. Two new generator concepts, based on DD technology, have been proposed. A pseudo-magnetic direct-drive (PDD) machine, integrating magnetic gearing and generator functions, may result in a significant weight reduction compared with PM-DD generators [1, 3]. In the EU project Innwind, relatively small PDD prototypes (5–16 kNm) were successfully designed, built and tested, but the concept remains to be proven in larger machines [4]. Furthermore, like PM-DD machines, PDD generators are subject to magnetic material prices, which significantly contribute to their levelized cost of energy. In addition, PDD generators have a complicated structure because of two rotating parts, making them difficult to be manufactured. In contrast, high-temperature superconducting (HTS) generators require only a small amount of rare-earth materials. Here, superconducting coils replace the PM rotor poles of a DD generator. Superconductors can carry high current densities, which results in power-dense low-weight coils with higher air-gap fields than in PM generators. Both HTS materials and cryogenic cooling technology have matured greatly over the last decade, making HTS electrical machinery not just technically feasible but also potentially economically competitive. Several projects have demonstrated this, albeit mostly in high-speed, low-torque machines [5–8]. The highest-torque machine successfully operated to date is a 36.5 MW, 120 rpm HTS propulsion motor by American Superconductor Corporation [9]. No HTS high-torque wind generator was manufactured prior to EcoSwing.

The EU H2020 EcoSwing project designed, developed and manufactured a full-scale 3.6 MW DD HTS generator, installing and operating it in an existing turbine. This demonstrated an advance of the technical readiness level (TRL) from 4–5 to 6–7 and the possibility to reduce the generator weight by 40%. The employed technology in principle also allows for higher power ratings than 3.6 MW. The EcoSwing consortium consists of nine partners from industry and academia:

- Envision Energy (Denmark) coordinated the project, provided the test turbine and was in charge of installation and commissioning on the turbine.
- Eco 5 (Germany) provided the core design.
- Jeumont Electric (France) manufactured the stator and assisted with both the rotor assembly and generator design.
- Delta Energy Systems (Germany) took care of the power converter and protection electronics.
- THEVA (Germany) delivered the superconducting wires and coils.
- Sumitomo (UK) supplied the cryogenic equipment.
- DNV GL (Germany) prepared certification procedures and guidelines for future installations.

- Fraunhofer Institute (Germany) ran a ground-based test; and
- University of Twente (Netherlands) tested the superconducting coils and assembled the rotor.

The main focus of this paper is the HTS rotor. However, first the general design of the entire generator is briefly reviewed in section 2, followed by a description in section 3 of the properties of the THEVA coated conductor that was used. In the coil design validation phase of the project, THEVA made several subscale coils that were tested at the University of Twente. The results—as well as the tests on the full-scale rotor coils—are described in section 4. In section 5 the cryogenic design and performance of the rotor is discussed in more detail. Jeumont 'married' the HTS rotor with the stator and shipped it to the Fraunhofer Institute for ground-based testing. Afterwards, the generator was installed on an existing wind turbine. The results of these ground-based tests and the operation in an existing turbine are briefly summarized in section 6. Lastly, conclusions are drawn in section 7.

2. General design

This section describes the main outline of the generator, more detailed design considerations are reported elsewhere [10]. In general, HTS generators can have either an air-core or iron-pole design, both for the conventional stator and superconducting rotor [11, 12]. Note that a fully superconducting generator (i.e. with also a superconducting stator, as proposed e.g. in [13]) was excluded early on in the EcoSwing design. For this first-of-its-kind demonstrator machine, the extra thermal load imposed by AC stator losses were deemed an unnecessary extra challenge. Furthermore, the rotor core can be kept either at cryogenic temperature ('cold rotor yoke') or at ambient temperature ('warm rotor yoke'). EcoSwing opted to design the generator as conservative as possible with a conventional stator and an HTS cold rotor with iron pole bodies. A major difference between EcoSwing and prior wind-related HTS projects is the full-scale in-field demonstration [14–16], which increases the TRL to 6–7. By involving a complete chain of suppliers for this demonstration, EcoSwing also increases the manufacturing readiness level to at least 6. However, this added several challenges to the design. First, for ease of transport, as well as to vacuum pressure impregnate the stator, the generator size needed to remain within a maximum diameter of 4 m. Second, the rotor's cryogenic cooling system needed to be as straightforward as possible. This lead to the choice not to use an actively cooled thermal radiation shield, to the use of single-stage cold-heads mounted directly in the rotating frame of reference and to the choice of conduction-cooling of the cold mass enclosed in one single large vacuum cryostat. More details about the cryogenic rotor design are given in section 5.

Since it needed to be installed in an existing turbine, the generator's axial length was limited to 2.5 m. Furthermore, the generator needed to have an efficiency higher than 92% in order to be competitive with PM-DD technology, as was

Table 1. Main specifications of the EcoSwing generator.

Generator design specifications	
Terminal power	3.6 MW
Rated speed	15 rpm
OD generator frame	4 m
Bearings	2 main
Free mechanical air gap	13 mm
Rated efficiency	∼92%
Stator type	Iron core sheets
Stator primary cooling	Radial air cooling
Stator voltage	710 V
Axial core length	1142 mm
Stator coils	Wound copper coils
Stator insulation	Mica insulation VPI class F
Electric loading	132 kA m^{-1}
Operation temperature rotor	<30 K
Rotor weight	30 t

**Table 2.** Main specifications of THEVA pro-line TPL2100.

THEVA Pro-Line TPL2100	
Tape width	12 mm
Thickness tape	0.21 mm
Copper thickness	100 μm
Minimum double bend diameter (RT)	60 mm
Maximum rated stress (RT)	300 MPa
Maximum rated tensile stress (77 K)	0.3%
Minimum I_c(77 K, SF)	250–360 A

installed on the turbine prior to the exchange. EcoSwing also aimed to demonstrate a 40% weight reduction of the generator, which could lead to a 25% reduction in the nacelle's weight. A list with the generator's key design features is given in table 1.

3. HTS conductor

THEVA provided the conductor for the field windings. Figure 1 shows the layered architecture of this HTS wire and table 2 summarizes its main specifications. The MgO buffer layer was grown using the inclined substrate deposition technique [17, 18]. This leads to a *c*-axis growth of the GdBCO layer under a tilt angle of ∼25°, which translates directly into the anisotropic behavior of the critical current density. Figure 2 shows this measured anisotropy for several batches of THEVA tape. The plot expresses the tape's critical current (I_c) in terms of a 'lift factor'. This lift factor is defined as the ratio between the critical current value under the expected operating conditions of the rotor ($T = 30$ K, $B = 1.5$ T) and the I_c value measured in liquid nitrogen and self-field ($T = 77$ K, $B = $ SF). The latter quantity is routinely acquired in-line by THEVA during tape production as part of their quality control program [19].

The University of Twente additionally measured the tape's performance at several magnetic fields (<1.5 T) and temperatures (20–50 K), analyzing the data with the
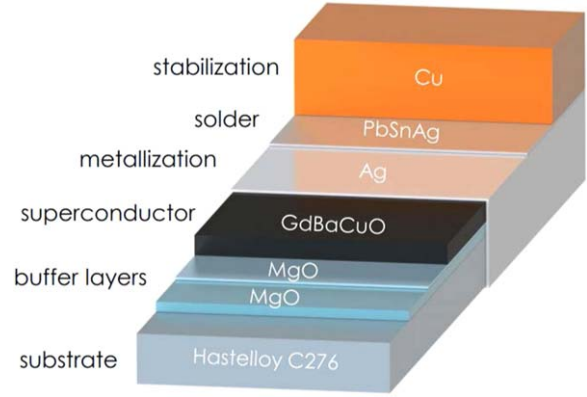
Figure 1. Schematic representation of THEVA's tape layered architecture. This includes: a Hastelloy substrate layer with a thickness of 95 μm, two MgO buffer layers ∼3.5 μm thick, the GdBaCuO film of ∼3.5 μm, a silver contact surround layer of ∼1 μm, PbSnAg solder and a 100 μm thick Cu laminated stabilization layer.
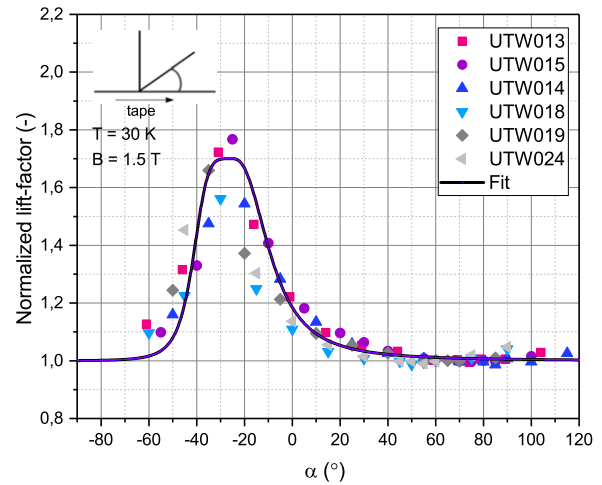
Figure 2. Measured normalized lift factor for several batches of THEVA tape as a function of the angle of the applied magnetic field. Also included is the fit from equation (1).

following 'scaling-law'. This expression follows a similar approach as first introduced by Fietz and Webb for low-temperature superconductors [20], which was later extended by Fleiter and Ballarino for HTS [21]

$$J_c(B, T, \alpha) = J_{c,c}(B, T) + \frac{J_{c,ab}(B, T) - J_{c,c}(B, T)}{1 + \left(\frac{\alpha + \beta}{g(B,T)}\right)^{\nu}}. \quad (1)$$

Here

$$J_{c,c} = \frac{a_c}{B} b_c^{p_c}(1 - b_c)^{q_c}(1 - t^n)^{\gamma_c}. \quad (2)$$

For a parallel applied field $\alpha = 0$. The *c*-axis shift of the THEVA tapes is accounted for by the angle $\beta = 25°$. Furthermore, $b_c = B/B_{i,c}$ and $t = T/T_c$ are the reduced field in perpendicular orientation and reduced temperature respectively, while g describes the anisotropy factor, corresponding to the angular half width at half maximum as shown in figure 2. Various parameters were simply adopted [21]
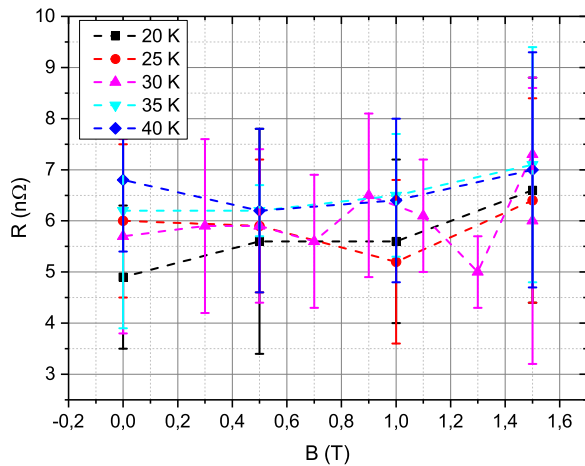
Figure 3. Measured resistance of the THEVA lap joint, with a 5 cm overlap, as a function of applied field for several temperatures.

because the critical surface was only sampled over a limited range around the envisaged operation point $T = 30$ K and $B = 1.5$ T. These fixed parameters were: $n = 1$, $q_c = 2.5$, $B_{i,c} = 140$ T, $T_c = 93$ K. Then the following parameters could be fitted: $g(B, T) = 17$, $Y_c = 1.96$, $p_c = 0.531$, $v = 2.5$, $a_c = 7.7 \times 10^{11}$ A T m^{-2} and $J_{c,ab}(B, T) = 1.7 J_{c,c}(B, T)$. This fit is included in figure 2 as a solid line.

The conductor's performance thus depends on the temperature, the magnetic field strength and the orientation of the field. The rotor's operational temperature should be stable below 30 K. However, the local magnitude and direction of the magnetic field experienced by the tape greatly varies throughout the winding pack of the coils. This means that varying tape quality can be used at different positions in the pole. In conjuncture with the tape production quality control information, this allowed increasing the overall production yield.

After verification of the lift factor on several batches, THEVA significantly scaled-up their production, reaching piece lengths 300 m and a monthly production capacity of up to 10 km. However, each rotor coil requires over 500 m of conductor, necessitating joints in the winding pack. After the development of a reproducible soldering process for low resistance joints of 'shaking-hand' type at THEVA, the University of Twente's setup was used to measure the resistance of the lap joint at several temperatures and magnetic fields, as shown in figure 3. This type of joint had an interface resistance of 36 ± 9 nΩ cm^{-2}, independent of temperature and field throughout the investigated range. At the generator's operating point, this corresponds to an acceptable dissipation level of $\sim$1 mW per joint.

4. HTS coils

4.1. Coil specifications

The HTS rotor-coil design was made according to the overall specification of the generator to achieve the desired power. Figure 4 shows an exploded view of the coil layout. Table 3
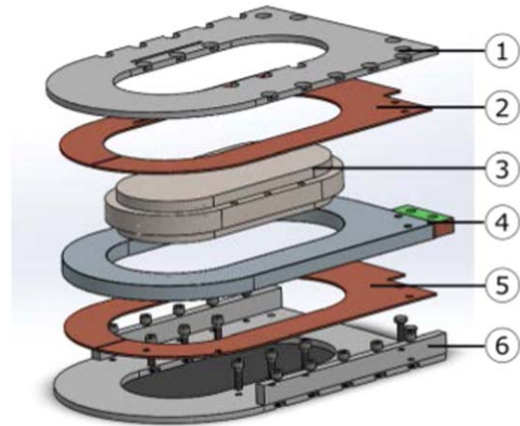
Figure 4. Explosion view of the subscale coil, which shows the main components: (1) top steel plate; (2) top copper plate; (3) iron-nickel core; (4) winding pack; (5) copper plate and; (6) bottom steel plate and side supports.

**Table 3.** Main specifications of the rotor coils.

EcoSwing rotor coil	
Geometry	Double-pancake
Length wire coil	>500 m
Length coil	~1400 mm
Lap joints	Up to 10
Insulation between turns	16 μm thick foil
Insulation between layers	25 μm thick foil
Insulation test	10 MΩ at 1 kV
Current connection	Two Cu connections at NDE
Weight winding pack	48 kg
TRL	7

lists its main specifications. The coils were co-wound—using HTS tape and a thin insulation foil—on a former, followed by a vacuum potting step with a two component resin and reinforced by glass roving lattice fabric. Copper plates, both on the top and bottom of the winding pack, form a thermal link for conduction-cooling the winding pack. At the generator's drive end (DE), these copper plates have a small slit to minimize eddy current losses. Furthermore, stainless steel plates (AISI 304 and 316) on the top, bottom and sides of the winding pack give the pole its mechanical strength. Finally, the pole assembly contains an iron-nickel core to strengthen and guide the magnetic field.

4.2. Testing of subscale coils

To validate this design, production started with a series of subscale coils. The radial layout (in the frame of reference of the generator) of these test poles reflected the actual layout of the full-scale rotor coils, but their axial length was significantly shorter ($\sim$330 mm instead of 1400 mm). The coils were mounted at the University of Twente in a vacuum chamber equipped with a two-stage cryocooler (Sumitomo Heavy Industries). The cryocooler's second stage was connected to the coil's copper plates to cool the winding pack. The setup could be controlled to stable temperatures between
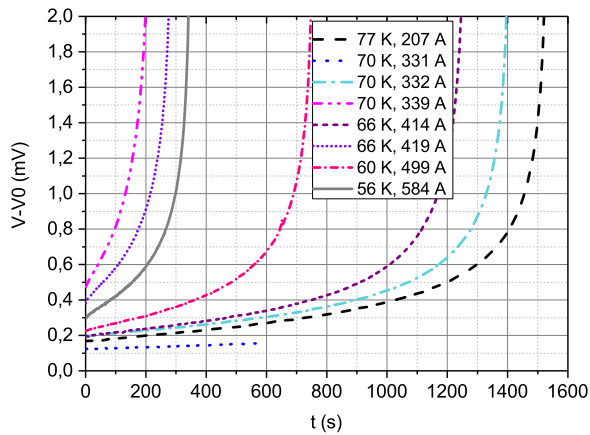
Figure 5. Thermal behavior of the subscale coil at different temperatures and currents plotted as voltage over time. The measurement at 70 K, 331 A was stopper after 600 s, because the coil's behavior was stable at this temperature and current. Thermal drift was observed at several current and temperature levels (below the critical values), showing that inadequate cooling results in a thermal quench.

Figure 6. Schematic of full-scale test rig, where: (1) top steel shell; (2) radiation shield; (3) aluminum table; (4) cryocoolers; (5) current feedthroughs; (6) coils and iron plates, shown in a four-coil configuration that was used for the acceptance tests; (7) bottom steel shell; and (8) turbomolecular pump backed up with a screw pump.

20 K and 80 K. The current leads were separated in two stages, so as to decrease the conductive heat load, which was further minimized by the use of HTS tapes. This design follows the general rules as described in [22]. To confirm the superconducting behavior of the coils, we measured their critical current as a function of temperature. This agreed well with the expected values. However, the measured n-values were relatively high (>100) at low temperatures, compared with the typical *n*-values (10–40) for HTS [23]. This suggests that the *I–V* transition, at least at low temperatures, is partially thermally driven.

Indeed, thermal drift leading up to eventual quenches has been observed in the conduction-cooled HTS coils. Here, a stable DC current was applied with a value below the coil's I_c. At first, the coil is still superconducting. However, over time the voltage across the coil increases in a gradually accelerating manner as shown in figure 5. This occurs at various currents and temperatures and will either stabilize over time or lead to a thermal runaway. Such thermal drifts have been reported earlier [24–26]. We investigated this behavior further and were able to describe it with a straightforward analytical model, which will be reported elsewhere. Although further coil testing and acceptance protocols could be adapted accordingly, it does stress the importance of an adequate thermal design in conduction-cooled HTS applications: even with a starting temperature well below the critical temperature, inadequate cooling may eventually result in a quench.

4.3. Testing of full-scale coils

After the coil design was validated with the subscale coil tests, a type-test on a full-scale rotor coil remained to be done. The larger axial length of the full-scale coils implies longer thermal paths, which could influence both the coil's electrical and thermal behavior. The relatively large size of the coils required a dedicated setup, which was used for the type-test as
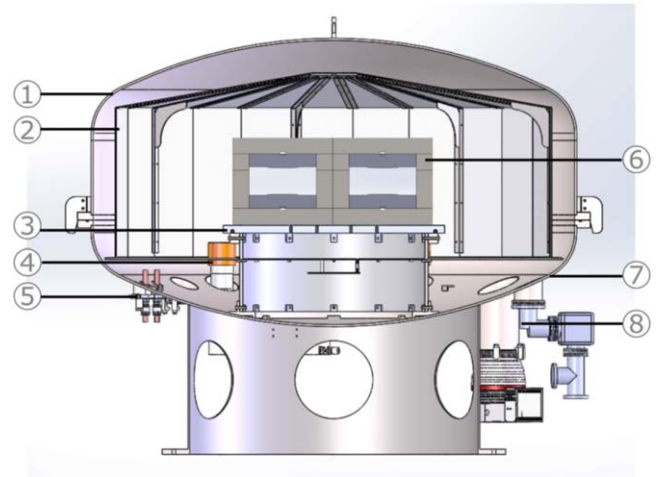
well as the acceptance tests of later coils (see below). Figure 6 shows a schematic cut-through of this test rig. The vacuum enclosure, made by Vernooy Vacuum Engineering, is a cylindrical steel shell that consists of two parts: a top lid and a bottom recipient. The base of this recipient rests on a thick-walled glass–epoxy cylinder that thermally insulates it from the ground whilst offering sufficient strength to support the weight. When closed, a turbomolecular pump (Leybold TURBOVAC T 450 i) backed up with a screw pump (Leybold LEUVAC 80) evacuates the enclosure to a pressure of 7×10^{-4} mbar in about 6 h. Inside the enclosure, an aluminum table holds up to four coils mounted in an iron cassette. With the aid of finite element modeling, the cassette is designed to mimic the magnetic environment that the coils experience in the generator. The general rotor layout and modeled EM environment are described in [10]. A copper tube is worked into the bottom of the aluminum table through which liquid nitrogen can flow to pre-cool the table. Two Giffhord-McMahon cryocoolers (SHI Cryogenics CH-110) cool the coils to temperatures between 30 K and 80 K. These coolers have a single-stage cold-head and are pressurized by water-cooled helium compressors, delivering a cooling power of 70 W at 30 K. Thermal insulation is provided by an adequate support structure, a vacuum enclosure and a radiation shield. For extra insulation, this aluminum shield is enveloped in multi-layer insulation (MLI) blankets and connected to an additional cryocooler. This same cryocooler also thermally anchors the current leads down to ∼60 K. From this 60 K copper bus to the 30 K coils, several THEVA tapes are implemented as an HTS current bridge to minimize conduction losses. Three 200 A power supplies are switched in parallel to excite the full-scale coils. These power supplies need to be used in 'voltage-control mode' to prevent excessive inductive voltage noise. Lastly, several voltage taps, hall-probes and temperature sensors monitor the behavior of the coil during testing. The voltage signals across the coils are
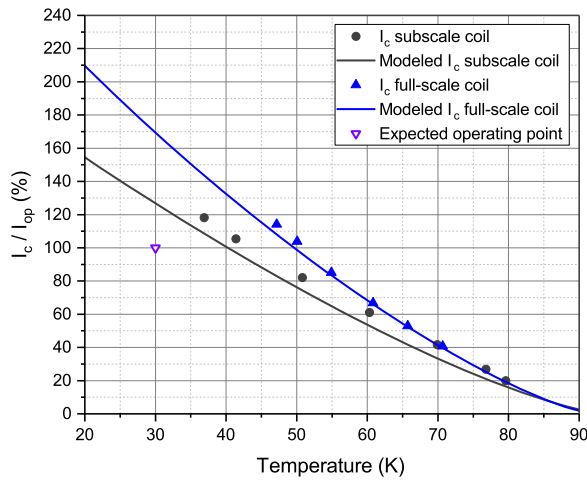
Figure 7. Measured I_c for both the subscale coil (gray dots) and the rotor coil (blue triangles) at various temperatures. Also included is the expected performance based on the tape's scaling-law and electromagnetic modeling of the coil. Furthermore, the purple triangle indicates the expected operating point of the rotor. Clearly, the rotor coil meets this criterion.

Figure 8. A schematic view of the EcoSwing generator.

connected to a quench detection system. When this system records an overvoltage, it opens an IGBT that feeds the current to the poles, thus forcing it to flow through a parallel dump resistor.

The test rig first allowed to type-test the full-scale rotor coil. Figure 7 shows the measured I_c values at several temperatures. Note that the performance of the full-scale rotor coil exceeds the subscale coil as the electromagnetic environment differs. This is also visible in the plot by the modeled performance of the two coils. Additionally, the rotor's expected operational point is indicated in the plot. The extrapolated critical current at these operating conditions exceeds this point, i.e. in the generator the coils are operated rather conservatively with a current margin of 70% and a thermal margin of 20 K. It was not possible to measure the I_c at this temperature due to limitations of the current leads. Repeated thermal cycles up to room temperature and back had no significant effect on the obtained I_c values. In addition, several thermal stability tests were done. At a set temperature of 30 K and 35 K, the current was kept stable first at elevated currents (up to ∼120% of the expected operating point for at least 2 h). If the coil would have been thermally unstable, the analytical thermal model discussed above predicts that temperature- and voltage drift should have been observed within these two hours. However, no such drift was observed and together with the other observations the HTS pole design was deemed amply validated.

4.4. Acceptance testing of full-scale coils

After confirmation of the coil's design, THEVA started with the series production of the 40 full-scale coils. As described above, the rotor coil test rig is adjustable to fit and test four coils simultaneously (powered in series). This was useful for the 'acceptance tests' of all coils. Since the rotor could only
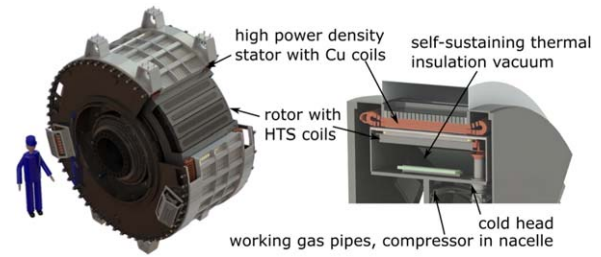
be tested after its vacuum enclosure had been welded shut, it was evacuated and its entire mass was cooled down, a substandard coil would lead to a lengthy repair procedure. Therefore, it was agreed to test all individual coils under similar conditions as the type-test described above. However, these tests are time-consuming, requiring roughly one week cool-down time for the entire cold mass (four coils plus iron cassette, together ∼1400 kg) and another four days to warmup. Since the coils are connected in series, failure of one also implied that the three other ones could not be tested properly and needed to be taken along in the next test run. In combination with the project's challenging time schedule, these issues impelled the project consortium to adopt a new acceptance test halfway through: an I_c-test in which only the 'bare' winding pack (impregnated but without pole piece or copper and steel plates) is immersed in liquid nitrogen. The drawback of this new test procedure is that the environment differs from that of the rotor—both thermally and magnetically. However, it did reduce the measurement time for four coils from two weeks to two days. With the tape's scaling-law (equation (1)) the minimum required I_c could be calculated. All coils reached this 77 K acceptance criterion. The risk of the 77 K test, with a different thermal- and magnetic environment, was accepted as the 30 K tests had shown that coils were either superconducting or not, i.e. rejected coils always showed ohmic features in their I–V curves even at low current. With these two acceptance tests, a coil yield of 91% was reached. In terms of the TRL of the HTS coils, this demonstrated an increase from level 4 to level 7.

5. Cryogenic rotor

Figure 8 shows a sketch of the whole generator, including the stator with its copper coils. For more detailed design considerations the reader is referred to [10]. The rotor consists of a warm central rim connected to the cold yoke where the HTS coils are attached to. These coils are thus inside a self-sustaining insulation vacuum, kept cold by nine cold-heads. In this section, technical details concerning the cryogenic rotor, including its assembly, will be discussed. ECO 5 did extensive computations of both the structural and dimensional integrity of this design. Assembly of the rotor was carried out by the University of Twente, at the premises and with assistance of Jeumont Electric.
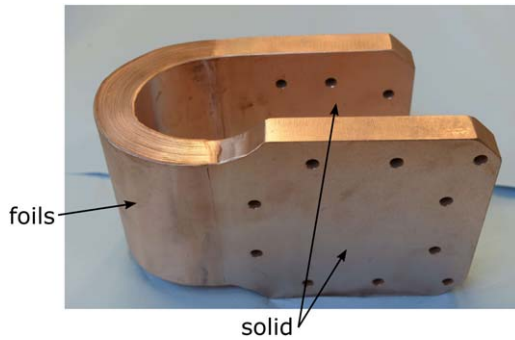
Figure 9. Photograph of the copper part between the cold-head and the thermal bus. It uses thick stacks of thin copper foils (the semi-circle) e-beam welded to solid copper parts (solid plates with holes for attachment) to allow for enough flexibility while maintaining proper mechanical strength.

5.1. Thermal circuit

The superconducting coils are the main critical component, requiring a temperature at or below 30 K to operate correctly. The 40 poles are bolted onto an FeNi9 cold yoke, with custom designed epoxy pads filling the gaps in-between the straight poles and the round yoke. Throughout the generator's cold mass, a purpose-developed mixture of MoS_2 and StyCast 1266 was used to tighten all structural bolts with a reproducible torque/force control and to secure them against loosening under vibrations. Compared to common commercial locking solutions, this mixture was experimentally found to provide a higher loosening torque at cryogenic temperatures. A ring-shaped oxygen-free high conductivity copper (Cu-OFE) 'cold bus' is attached to the yoke's non-drive end (NDE). This bus is not an uninterrupted ring, but divided into four quadrants, both for ease of machining/handling and to prevent excessive induced currents due to asymmetries in the generator's stray field. The cold bus is connected to the copper cooling plates of the individual coils through flexible copper connectors. These thermal links consist of thick stacks of ~100 0.2 mm thin Cu-OFE foils that were e-beam welded to solid copper end-parts, as shown in figure 9. This solution accommodates both differential thermal contraction of the rotor's components and the expected mechanical vibrations in operation. Similar links are placed between the cold bus and the rotating GM cold-heads (Sumitomo RDK-500B). Sample pieces that were spark-eroded from the Cu-OFE pieces revealed that the machined material had an RRR value of ~80, which—presumably due to work hardening—is on the low side for this purity grade. Therefore, prior to assembly all pieces were vacuum- or nitrogen-annealed for 12 h at 350°C. This protocol was empirically established to yield the optimal balance between final RRR value (~170) and Vickers hardness. All thermal interconnects between copper parts were realized using clamped contacts with thermal grease in-between (Apiezon N) to maximize the contact area. For electrical copper-to-copper contacts, a different strategy was used (see section 5.2).

The cold yoke is mechanically connected to the warm central rim through several specifically designed cold-warm-
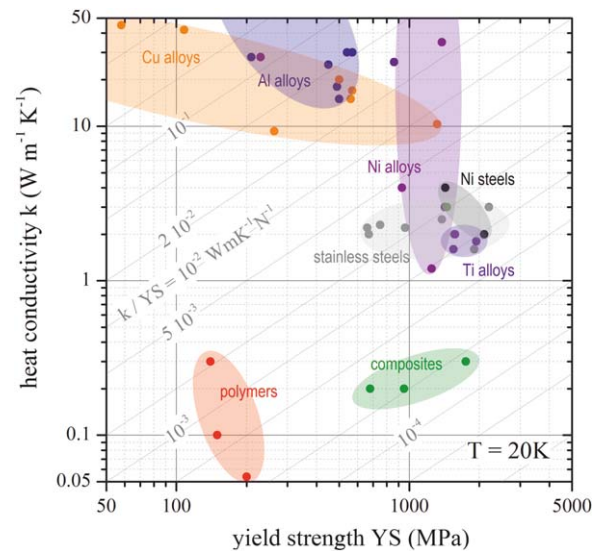
Figure 10. Heat conductivity as a function of yield strength for various materials at a temperature of 20 K. Compiled from data in [27, 28].

Figure 11. Photograph of one subscale CWS that was mechanically load tested with one side at room temperature and the other in liquid nitrogen.

supports (CWS). These need to transfer the considerable torque exerted by the wind turbine that is connected to the rim, while simultaneously minimizing the heat load on the yoke. As illustrated by figure 10, glass-fiber reinforced polymer plates, with reported yield stress ranging from 500–2000 MPa, are ideal for this [27, 28]. Mechanical load testing of subscale test coupons, with one side at room temperature and the other in liquid nitrogen, was done

Figure 12. A picture of the cold-heads with sock enveloped in three layers of MLI.

(figure 11). The coupons, with 1/7 width of the CWS and similar end fixations, survived tensile and compressive loads >2 times the peak nominal design load of ∼20 MPa without yielding, with signs of irreversible degradation only setting in at four times this peak load. Note that the cited design stresses are nominal values in the main body of the plate. Yielding actually starts at the plate fixtures, where stress concentration occurs. Interestingly, the warm side of the coupons degraded first. Furthermore, an accelerated fatigue testing program designed to model generator-relevant load profiles revealed no significant evolution of the coupons' mechanical properties.

In total, eight cold-heads cool the expected heat load. Using the experience gained with the full-scale coil test rig (section 4), one extra cold-head is dedicated for cooling of the current leads. The cold-heads' performance, i.e. their delivered cooling power, depends on their angular orientation. This influences the coils' temperatures. Furthermore, the cold-heads need to be accessible for maintenance without having to warm-up the rotor. Therefore, Sumitomo employed a 'sock' design that allows decoupling a cold-head from the large cold mass during servicing. This sock, a picture is shown in figure 12, seals the main vacuum and has its own insulation vacuum. The long-term quality of the vacuum is ensured by adding charcoal adsorption material to the inside. Sumitomo thoroughly tested this technique by repeatedly disconnecting and connecting a cold-head without degradation of the thermal contact.

While the cold-heads are mounted on-board the rotor, the water-cooled compressors (F70-H) remain stationary. These nine compressors feed a helium high-pressure line that transfers to the cold-heads through a rotary joint assembly (RJA). A sketch is given in [10]. The RJA serves both as feedthrough for electrical power and signals (slip ring system) as for the high- and low-pressure He flow. This latter functionality is based on a commercial feedthrough for gases,

adjusted for use with helium. The design was adjusted by Sumitomo in such a way that two outer low-pressure lines protect the high-pressure line against ambient pressure. This lowers the risk both of He loss and of contamination.

5.2. Excitation circuit

The DC current in the rotor coils is furnished by a commercial supply mounted on the warm rotor hub. Power to this supply is fed in through the slip ring assembly (which also takes out the various measured signals as described in section 5.3).

One cold-head is dedicated to cool the current leads used for excitation. A purpose-built cryogenic heat-exchanger thermally anchors the leads directly to this cold-head. This heat-exchanger basically consists of a copper box with the current leads running through, galvanically separated from the box and from each other with thin fiber-glass sheets. All successive coils are connected anti-series through coil-to-coil connectors with a hybrid copper-HTS design, which have an average resistance of 32 nΩ at 77 K. Custom-made cotton-phenolic covers isolate and protect all these bridges. Throughout the rotor, electrical copper-to-copper connections are clamped together with soft indium wire in-between to maximize the contact interface and thus to minimize the resistance. This necessitated a procedure in which the clamping bolts were repeatedly tightened to allow the indium to gradually creep to its final thickness (typically in three to five tightening steps spread over several days). This creep process was monitored by each time logging the bolts' angular position at a controlled tightening torque.

5.3. Instrumentation

The rotor contains various sensors, including 68 carbon ceramic sensor thermometers (CCS). These sensors are robust, relatively insensitive to magnetic fields and can withstand high mechanical forces and vibrations [29]. Each coil contains one CCS. Additional CCS sensors are on the cold yoke, on the cold bus, on the current bus and on selected CWS. Two 'heavily-instrumented' coils are, besides these CCS sensors, equipped with extra CERNOX-type temperature sensors and hall-probes. Furthermore, voltage taps are placed along the excitation circuit. These voltage taps span groups of four coils and are monitored by purpose-designed DAQ cards mounted on the warm rotor hub for quench detection purposes. Surge-suppressing resistors, placed in series with the voltage taps and thermally anchored, limit possible fault currents that might jeopardize the detection electronics during a quench. The quench protection strategy is based on both voltage and temperature signals. Essentially, the quench detection cards evaluate the coil group voltages differentially against neighboring sets of coils in order to minimize inductive contributions. Like with the full-scale coil test rig described above, in case of a quench the IGBT that furnishes the excitation current blocks, dumping several MJ of stored energy in a parallel shunt resistor. For all sensors Teflon-coated 4-lead wire was used, combining adequate electrical insulation and mechanical robustness. The voltage
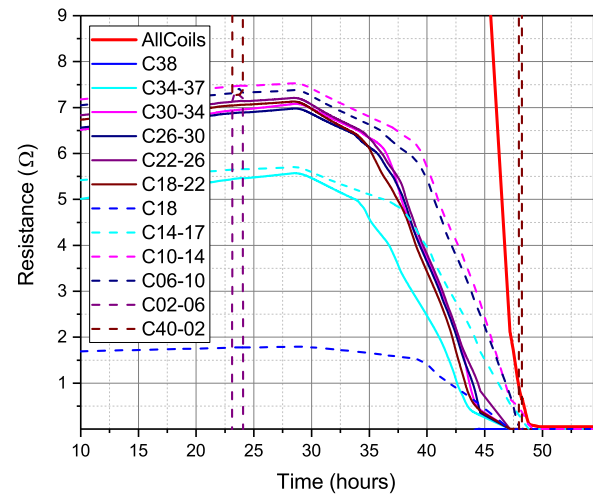
Figure 13. Photograph of the EcoSwing rotor enveloped in three MLI blankets.


Figure 14. Measured voltages across the groups of four coils as a function of time. This was measured at a constant current of 0.1 A. It shows the sudden decrease of the resistance, which is typical for a normal–superconducting transition.

leads were twisted in pairs as close to the attachment points as possible and also pulled through Teflon sleeves. In view of the expected mechanical vibrations of the generator, all wiring was carefully routed along and regularly tied to dedicated wire guides and then along the NDE of the CWS to the warm hub.

41-pins commercial vacuum feedthroughs are used for the sensor wiring. For the current feedthroughs a dedicated design was realized. The leak rate of this design is less than 5×10^{-11} Pa m^3 s^{-1}. The stainless steel vacuum chamber itself was manufactured using explosion bonding, its radially outer mantle was copper-clad on the vacuum side to act as an electromagnetic damper. Before positioning the rotor into the chamber, the coils, cold yoke and current bus were enveloped in three MLI blankets (Coolcat 2NW) (figure 13). Underneath the MLI, a robust but flexible layer of Tyvek cloth was draped over the entire yoke (i.e. on top of all poles, sensors, wiring, etc), protecting the relatively fragile MLI from rubbing and tearing at protruding parts (e.g. bolt heads or pole corners). The poles and yoke on the NDE side were covered by an additional strip of insulation material (aluminum and glass-fiber cloth, type CoolCat H) in order to protect the underlying MLI blankets from heat during the welding-shut of the vacuum chamber. The rotor was then lowered into the chamber and the axial end-flanges were welded on. As a standard preliminary control, all welds were verified with a die penetration method.

5.4. Vacuum

Once closed, the chamber was vacuum leak-tested. Evacuation with only the fore-pump caused the pressure to fall to $\sim$50 Pa within 24 h, which is well within expectations. The leak rate of the chamber was well below 10^{-9} Pa m^3 s^{-1}. Already in the design phase, it was decided that the rotor must allow replacements of components after testing. Thus it had to be possible to open and close the vacuum chamber for repairs and the welding surfaces were designed accordingly. This choice proved to be fortuitous, since testing at the Fraunhofer

Institute for Wind Energy and Energy System Technology (IWES) revealed one sub-standard pole that had passed the accelerated acceptance test at 77 K, but nevertheless at 30 K had a lower I_c value than required. Therefore, after the IWES test the vacuum chamber was cut open again and the coil was replaced. After re-welding the chamber shut, it reached a base pressure of 2.7×10^{-5} Pa.

6. Generator test results

After completion of the rotor's assembly, JEUMONT 'married' the superconducting rotor with a purpose-designed and -manufactured stator. The generator was then shipped to IWES for detailed testing. After completion of these tests and the repair mentioned above, the generator was installed on an existing modern wind turbine in Thyborøn, DK. A more detailed description of these tests results will be published elsewhere [30], in this section we provide a summary of the rotor-related highlights.

While the test bed at IWES was prepared, the superconducting rotor was cooled down. During cool-down a small current was applied to the HTS coils to monitor their resistive transition. The cool-down to stable temperatures took 14 d, which is $\sim$1/4 faster than the model prediction of 18 d. This period also included several interruptions to lift of the generator onto the test bench. The final coil temperatures ($\sim$20–22 K) were significantly below the target temperature (30 K) and all coils showed the typical superconducting–normal transition (figure 14). Moreover, the temperatures remained below 30 K even when three compressors stopped. This better-than-designed cooling performance improved further during rotation. At $\sim$15 rpm the equilibrium temperatures dropped further by 2.5 K compared to their values at standstill. Also the temperature differences among the 40 coils decreased during rotation. Both effects occur due to the
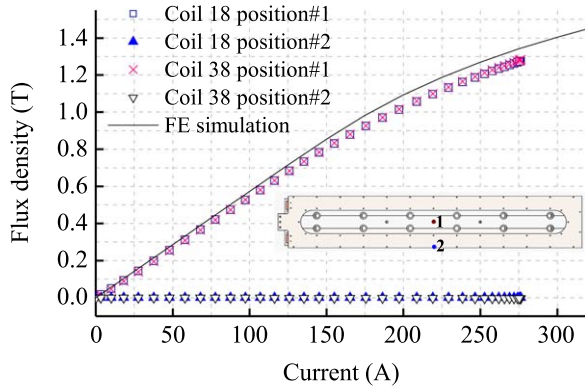
Figure 15. Measured magnetic field from the hall-probes on the heavily-instrumented coils as a function of the applied current. The measured data (points) match well (within 10%) with the model (black line). Also included is a sketch with the locations of the sensors.

Figure 16. Temperature (left axis) and voltage (right axis) of the sub-standard coil as a function of the applied current during the excitation, no rotation tests. Both voltage and temperature signals increase drastically around 220 A, which indicates that this coil had a lower I_c than required from the start.

orientational dependence of the cold-heads' efficiency. Together, all these observations indicate that the cryogenic design is amply adequate and can be considered as conservative.

The first excitation of the rotor was carried out in steps. First, the rotor was excited at a standstill. Figure 15 shows the measured magnetic field of two hall-probes (located on the iron pole of the heavily-instrumented coils) plotted against rotor-current. The data match well with the design expectations, within 10%. Clearly, the obtained fields are higher than the practical limits that can be achieved with either copper wound-rotor ($\sim$0.8 T) or with PM-technology ($\sim$1 T). Under rotation, EM inductive interference significantly increased the voltage noise, even leading to clipping of the DAQ signals. This spurred a re-adjustment of the quench detection cards after the IWES tests, increasing their range and adapting the filtering strategy. Still at IWES, at about 280 A (with $\sim$15 rpm rotation) a sudden voltage rise triggered the quench protection system. During this event the temperature of one coil continued to increase for several minutes, with a maximum recorded temperature rise of 4 K. This indicates that this coil quenched around 280 A. Resistive measurements of the coil after the quench showed that the coil got permanently damaged. This is most likely due to the high threshold of the quench detection system, necessitated by the voltage noise, making the system too slow to react and prevent damage to the quenched coil. Yet, even with the damaged coil, the rotor could still carry a stable current of 130 A. Therefore, it was possible for the generator to produce power under partial load, resulting in a 1 MW delivered output power.

Post-processing the data revealed that the coil that quenched showed characteristics of a lower I_c than required—already during the standstill situation. Figure 16 shows both the measured temperature and voltage data as a function of the applied current. Around 220 A both the voltage and temperature signals increase faster indicative of a super-conducting–normal transition. This implies that this rotor coil already had a lower I_c before the quench event. Moreover, this rotor coil was tested in liquid nitrogen only. The lower I_c was
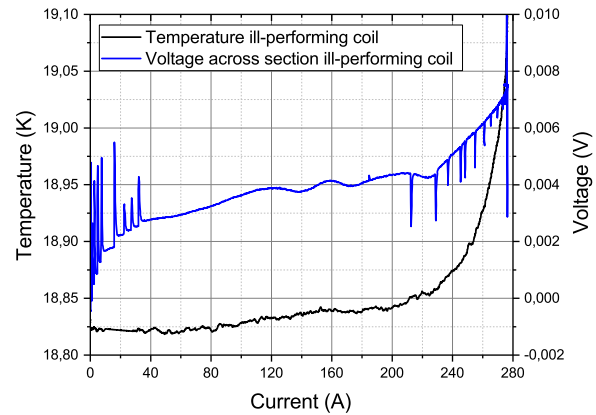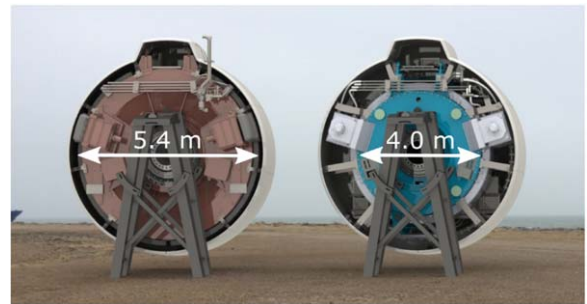
Figure 17. Picture of the EcoSwing generator with a diameter of 4 m next to the previously installed PM generator with a diameter of 5.4 m.

not seen during these acceptance tests. All other coils did not show this thermal runaway behavior during the testing period at IWES. Various coils did increase slightly in temperature, but all—except the quenched coil—stabilized over time.

The sub-standard coil was replaced after the testing period at IWES (see section 5). The generator was then shipped to a coastal site in Western Denmark, Thyborøn and operated in-field. Figure 17 shows the generator next to the previously installed PM generator with same power rating. At Thyborøn the generator reached its target range and produced power to the grid for more than 650 h. In total, the cryogenic system behaved stable for more than 7 months.

7. Conclusion

The EcoSwing project successfully designed, developed, manufactured and field-tested a full-size superconducting generator for a 3.6 MW wind turbine. This required a major impact on quality and stability of HTS wire manufacturing capability. The production capability jumped from meters per week to kilometers per week. This was also accompanied with a substantial upscale of HTS coil production; more than

40 poles were produced with a pole yield of >90%. It demonstrates that HTS coil production is not limited to specialized laboratories and constitutes a successful technology transfer from science to industry. Furthermore, also the HTS rotor assembly was performed in an industrial setting, showing that superconducting components can be deployed in such a 'standard' manufacturing environment. Prior wind-related HTS projects did not involve a complete chain of suppliers or an in-field demonstration.

Ground-based and in-field testing of the generator resulted in more than half a year of problem-free cryogenic operation. The cold rotor reached a base pressure of 2.7×10^{-5} Pa, which was re-established after a repair involving the replacement of one sub-standard coil. This sub-standard coil was identified during a quench at IWES, while the coil had passed the accelerated acceptance test. Adequate coil testing has thus been identified as an important de-risking effort within the project. Additionally, quench detection was found to be extra challenging in environments with high EM inductive interference. Hence, after the ground-based tests the quench protection system was upgraded prior to the installation of the generator in the wind turbine at Tyborøn. At Thyborøn all coils behaved as expected and the turbine achieved its targeted power range including more than 650 h of grid operation. This demonstrates the compatibility of superconductive generator technology with all the real impacts present in an operational environment such as variable speeds, grid faults, electromagnetic harmonics, vibrations etc. In doing so, EcoSwing has lifted the technology for superconductive generators to TRL 7.

Acknowledgments

ORCID iDs

Anne Bergen ⓘ https://orcid.org/0000-0002-0422-5560
Xiaowei Song ⓘ https://orcid.org/0000-0001-8051-5474

References

[1] Polinder H, Ferreira J A, Jensen B B, Abrahamsen A B, Atallah K and McMahon R A 2013 Trends in wind turbine generator systems *IEEE J. Emerg. Sel. Top.* **1** 174–85

[2] Spinato F, Tavner P J, Van Bussel G J W and Koutoulakos E 2009 Reliability of wind turbine subassemblies *IET Renew. Power Gener.* **3** 387–401

[3] Moore S K 2018 Rough seas for the superconducting wind turbine *IEEE Spectrum* **55** 8

[4] Jensen P H et al 2017 *LCOE reduction for the next generation offshore wind turbines* Outcomes from the INNWIND.EU project

[5] Frank M, Frauenhofer J, van Hasselt P, Nick W, Neumueller H W and Nerowski G 2003 Long-term operational experience with first Siemens 400 kW HTS machine in diverse configurations *IEEE Trans. Appl. Supercond.* **13** 2120–3

[6] Kalsi S S, Gamble B B, Snitchler G and Ige S O 2006 The status of HTS ship propulsion motor developments *IEEE Power Engineering Society General Meeting* (https://doi.org/10.1109/PES.2006.1709643)

[7] Fair R, Lewis C, Eugene J and Ingles M 2010 Development of an HTS hydroelectric power generator for the Hirschaid power station *J. Phys.: Conf. Ser.* **234** 032008

[8] Sivasubramaniam K, Zhang T, Lokhandwalla M, Laskaris E T, Bray J W, Gerstler B, Shah M R and Alexander J P 2009 Development of a high speed HTS generator for airborne applications *IEEE Trans. Appl. Supercond.* **19** 1656–61

[9] Gamble B, Snitchler G and Macdonald T 2011 Full power test of a 36.5 MW HTS propulsion motor *IEEE Trans. Appl. Supercond.* **21** 1083–8

[10] Song X et al 2019 Designing and basic experimental validation of the world's first MW-class direct-drive superconducting wind turbine generator *IEEE Trans. Energy Convers.* accepted (https://doi.org/10.1109/TEC.2019.2927307)

[11] Lewis C and Müller J 2007 A direct drive wind turbine HTS generator *IEEE Power Eng. Soc. Gen. Meeting* (https://doi.org/10.1109/PES.2007.386069)

[12] Frauenhofer J, Grundmann J, Klaus G and Nick W 2008 Basic concepts, status, opportunities, and challenges of electrical machines utilizing high-temperature superconducting (HTS) windings *J. Phys.: Conf. Ser.* **97** 012189

[13] Haran K S et al 2017 High power density superconducting rotating machines—development status and technology roadmap *Supercond. Sci. Technol.* **30** 1230

[14] Magnusson N, Eliassen J C, Abrahamsen A B, Nysveen A, Bjerkli J, Runde M and King P 2015 Design aspects on winding of an MgB$_2$ superconducting generator coil *Energy Procedia* **80** 56–62

[15] Song X et al 2017 A full-size high-temperature superconducting coil employed in a wind turbine generator setup *IEEE Trans. Appl. Supercond.* **27** 7828024

[16] Sarmiento G, Sanz S, Pujana A, Merino J M, Marino I, Tropeano M, Nardelli D and Grasso G 2016 Design and testing of real-scale MgB2 coils for SUPRAPOWER 10-MW wind generators *IEEE Trans. Appl. Supercond.* **26** 7397945

[17] Quinton W A J and Baudenbacher F 1997 Deposition of biaxially aligned YSZ films on inclined polycrystalline metallic substrates for YBaCuO tapesm *Physica* C **292** 243–7

[18] Bauer M, Semerad R and Kinder H 1999 YBCO films on metal substrates with biaxially aligned MgO buffer layers *IEEE Trans. Appl. Supercond.* **9** 1502–5

[19] Furtner S, Nemetschek R, Semerad R, Sigl G and Prusseit W 2004 Reel-to-reel critical current measurements of coated conductors *Supercond. Sci. Technol.* **17** S281–4

[20] Fietz W A and Webb W W 1969 Hysteresis in superconducting alloys–temperature and field dependence of dislocation pinning in Niobium alloys *Phys. Rev.* **178** 657–67

[21] Fleiter J and Ballarino A 2014 Parameterization of the critical surface of REBCO conductors from Fujikura *CERN Internal Note* 2014-24, EDMS No. 142639

[22] Chang H M and Van Sciver S W 1998 Thermodynamic optimization of conduction-cooled HTS current leads *Cryogenics* **38** 729–36

[23] Iwasa Y 2009 *Case Studies in Superconducting Magnets: Design and Operational Issues* (Boston: Springer) (https://doi.org/10.1007/b112047)

[24] Vysotsky V S *et al* 2000 Thermal quench study in HTSC pancake coil *Cryogenics* **40** 9–17

[25] Miyazaki H, Iwai S, Tosaka T, Tasaki K, Hanai S, Urata M, Ioka S and Ishii Y 2011 Thermal stability of conduction-cooled YBCO pancake coil *IEEE Trans. Appl. Supercond.* **21** 2453–7

[26] Umans S D, Shoykhet B A, Zevchek J K, Rey C M and Duckworth R C 2007 Quench in high-temperature superconducting motor field coils: experimental results at 30K *IEEE Trans. Appl. Supercond.* **17** 1561–7

[27] Campbell J E, Eldridge E A and Thompson J K 1974 Handbook on materials for superconducting machinery *US National Technical Reports* 197504

[28] Ekin J 2006 *Experimental Techniques for Low-Temperature Measurements* (Oxford: Oxford University Press)

[29] Datskov V, Kirby G, Bottura L, Perez J C, Borgnolutti F, Jenninger B and Ryan P 2013 Precise thermometry for next generation LHC superconducting magnet prototypes *IEEE Trans. Appl. Supercond.* **24** 6656885

[30] Song X *et al* 2019 Ground testing of the world's first MW-class direct-drive superconducting wind turbine generator *IEEE Trans. Energy Convers.* submitted